Check for updates

Nanoparticle-based colorimetric biosensor for the detection of telomerase activity based on the peroxidase-mimicking activity of nanogold

Le Thi Hoang Uyen,[ab] Vo Thi Cam Duyen[ab] and Phuoc Long Truong ᴵᴰ *[ab]

The early detection of cancers can be done by monitoring telomerase activity as it is considered a cancer biomarker. Several strategies for detecting telomerase have been developed, including polymerase chain reaction (PCR)-based and PCR-free assays. Despite various advantages of these strategies such as high sensitivity and accuracy, they have many limitations such as being time consuming and labor-intensive; they are also prone to provide false negatives and unsuitable for onsite testing. This study suggests a simple, fast, and low-cost method for the ultrasensitive detection of telomerase by exploiting the selective cleavage of exonuclease III and catalytic activity of nanogold. In the presence of telomerase, the primer is elongated and hybridized with its complementary strand, resulting in the formation of dsDNA with a blunt end. The dsDNA is then cleaved by exonuclease III to release the elongated primers. Once released, these primers get adsorbed on nanogold and suppress its catalytic activity. In the absence of telomerase, exonuclease III completely digests the dsDNA, resulting in the uninhibited catalytic activity of nanogold that can oxidize TMB into a blue-colored product. The proposed method enabled the detection of telomerase in 100 MCF-7 cells by the naked eye. Absorbance measurements revealed a detection limit of $\sim$0.3 MCF-7 cells with a wide linear range from 10^2 to 10^6 cells. This sensing approach provided a simple PCR-free method for the detection of telomerase with high sensitivity and specificity, demonstrating its potential utility as a proof-of-concept platform for telomerase-related cancer research, with future diagnostic development contingent upon further validation.

1 Introduction

Telomerase is known as a crucial ribonucleoprotein enzyme in eukaryotic cells, which plays a significant role in maintaining telomere stability, cellular immortalization, and cancer progression. Telomerase functions as a telomere terminal transferase, elongating the ends of chromosomes by reverse transcription with its own RNA template.[1,2] The underlying mechanism is that telomeric repeats (TTAGGG) are attached onto the 3′-end of chromosomes, which then prevent the progressive shortening of telomeres during the cell division cycle. The activity of telomerase is mostly found in the stem cells, reproductive cells, and cancer cells in humans, in which it assists in the cell proliferation and maintenance of telomeres.[3] Telomerase dysregulation has been linked with cancer development and progression. Almost all human cancer cells possess short telomeres and a high telomerase activity level, allowing for the uncontrollable cell division and growth of tumors.[4] Telomerase overexpression can be observed in 80–90% of malignant cases in humans. To be more specific, malignant cells overexpress human telomerase reverse transcriptase (hTERT) and the catalytic protein, telomerase ribonucleoprotein (RNP), highlighting the correlation between telomerase activity and tumorigenesis.[5] Furthermore, studies have shown that telomerase malfunction is linked to a variety of illnesses including cancer, premature aging syndromes, and age-related disorders, emphasizing its potential as a biomarker for disease diagnosis, prognosis, and monitoring.[6] To fully realize the diagnostic and prognostic potential of telomerase, improved analytical approaches for the sensitive, rapid, and reliable detection of telomerase activity in clinical samples are necessary.[7] Currently, the telomeric repeat amplification protocol (TRAP) traditionally serves as the gold standard for assessing telomerase activity. Besides the advantages of this method, such as ultra-sensitivity, a wide dynamic range, repeatability, and accuracy, it still has several limitations associated with the amplification step. These include being time-consuming, difficult to quantify precisely, prone to amplification-related artifacts (*e.g.*, nonspecific products or primer–dimer formation), and relatively costly.[8,9] To address these limitations, various PCR-free assays for telomerase analysis have been developed, such as the peroxidase-mimicking catalytic activity of DNAzyme,[10] CRISPR-Cas12a-based assays,[11] telomeric hemin/G-quadruplex-induced agglomeration of

ᵃSchool of Biomedical Engineering, International University, Ho Chi Minh City 700000, Vietnam. E-mail: tplong@hcmiu.edu.vn

ᵇVietnam National University, Ho Chi Minh City 700000, Vietnam

colloidal nanoparticles,[12] and electrochemical sensing.[13,14] Nevertheless, each method has its own shortcomings for practical application in clinical diagnostics, such as complexity, high cost, time-consuming, requirement of elaborate apparatus, and inability to perform point-of-care testing. For these reasons, there is a great demand for the development of a simple, fast, cost-efficient, accurate, and quantitative PCR-free assay for telomerase analysis.

In recent years, nanotechnology has emerged as a promising avenue for developing novel sensing platforms that overcome the constraints of conventional analytical approaches.[15] Plasmonic nanoparticles, characterized by their unique optical properties and biocompatibility, offer an attractive platform for colorimetric biosensors capable of detecting biomolecules with simplicity, rapidity, high sensitivity and specificity with a small amount of reagents for testing.[16] The sensing mechanism of these colorimetric biosensors is mainly based on the alteration in the color of colloidal nanoparticles due to their target-induced aggregation *via* various interactions, enabling the simplified, cost-effective, on-site and practical detection of analytes.[17–21] For telomerase detection, most studies exploit DNA-functionalized Ag/Au nanoparticles and nanoprobes constructed *via* Au/Ag–thiol bonding interactions. However, the process for the functionalization of metallic nanostructures is time-consuming, and it is essential to optimize the amount of DNA molecules loaded on the nanoparticle surface before telomerase sensing, block the nanoparticle surface to reduce non-specific binding and minimize the steric hindrance at the binding site of DNA on the nanoparticle surface. Moreover, DNA-conjugated nanoparticles that suffer from the degradation by various nucleases can lead to unexpected false-positive signals of assays.[22,23] In clinical applications, complex biological environments can affect the stability of DNA nanoprobes used for telomerase analysis in clinical samples. In recent studies, noble metallic nanoparticles were reported to possess intrinsic peroxidase-like catalytic activity, which can convert the colourless substrates of peroxidase into coloured reaction products, and this catalytic activity can be tuned by functional molecules such as proteins, aptamers and antibodies. More recently, studies have discovered that the peroxidase-like catalytic activity of metallic nanoparticles can be suppressed by blocking their surface with single-stranded DNA *via* electrostatic absorption, which can induce a shielding effect against the catalytic activity of nanoparticles, and this shielding effect has been utilized to develop novel sensing platforms for the colorimetric detection of glucose, protein, DNA and heavy metals.[24–26]

In this work, we present a novel PCR-free method for the colorimetric measurement of telomerase activity, which plays an important role in cancer diagnosis. The proposed sensing approach exploits the telomere extension activity of telomerase coupled with the specific cleavage of exonuclease III and switchable peroxidase-like catalytic activity of colloidal gold. Compared to prior methods for the detection of telomerase activity, the current sensing approach enables the simple, reliable, ease-of-use, straightforward detection of telomerase activity with improved sensitivity and specificity. The whole assay can be conducted within ~3 hours in a label-free manner and it does not need costly equipment. Furthermore, the colorimetric response of the nanosensor can be detected by the naked eye or a low-cost portable spectrophotometer. Hence, this sensing method may lay the groundwork for the development of an easy-to-use and low-cost telomerase assay, providing a proof-of-concept platform that could be further adapted for on-site analysis following validation in complex clinical samples. The features of the proposed sensing approach are advantageous compared to traditional PCR methods and other PCR-free methods.

2 Experimental

2.1 Materials

3-[(3-Cholamidopropyl)dimethylammonio]-1-propanesulfonate (CHAPS) hydrate was purchased from Bio Basic Inc. (Canada). Gold(III) chloride trihydrate ($HAuCl_4 \cdot 3H_2O$, 99.9%), trisodium citrate, sodium chloride (NaCl), potassium chloride (KCl), magnesium chloride ($MgCl_2$), phosphate-buffered saline (pH 7.4), UltraPure™ tris hydrochloride, 3,3′,5,5′-tetramethylbenzidine (TMB, 99%), hydrogen peroxide (H_2O_2), Dulbecco's modified Eagle medium (DMEM), fetal bovine serum (FBS), ethylenediaminetetraacetic acid (EDTA) and penicillin-streptomycin-neomycin (PSN) solution were purchased from Sigma-Aldrich, Inc. The oligonucleotide sequence utilized for telomerase extension (TS primer: 5′-AAT CCG TCG AGC AGA GTT-3′), the TS complementary sequence (TS complementary: 5′-AAC TCT GCT CGA CGG ATT-3′), dNTPs (dATP, dGTP, dCTP, and dTTP mixture) and agarose were obtained from PHUSA Biochem Co., Ltd (Can Tho City, Vietnam). Exonuclease III was supplied by Thermo Fisher Scientific. Tris-acetate-EDTA (50×) was purchased from ABT (Vietnam). Hydrochloric acid (HCl), sodium hydroxide (NaOH, 99%) and nitric acid (HNO_3) were purchased from Xilong Scientific Co., Ltd (China). Normal human fibroblast cells, mouse fibroblast cells (L929), human breast adenocarcinoma cells (MCF-7), mouse colon carcinoma cells (C26) and human liver cancer cells (HepG2) were purchased from ATCC (USA). All glassware was treated with an aqua regia solution and washed several times with distilled water. All tubes and pipette tips were treated with 0.1% solution of diethylpyrocarbonate (DEPC) overnight to inactivate RNases before use. DEPC-treated water was used to prepare all solutions for experiments.

2.2 Preparation of cell extracts from cultured cells

The preparation of cell extracts using CHAPS lysis buffer was adapted from a previous study by Huyen *et al.* (2025), with minor modifications to accommodate the nanozyme-based readout employed in this study.[33] MCF-7 human breast adenocarcinoma cells, normal human fibroblast cells, mouse fibroblast cells (L929), mouse colon carcinoma cells (C26), and human liver cancer cells (HepG2) were cultured in Dulbecco's modified Eagle medium (DMEM) containing 10% fetal bovine serum (FBS) at the temperature of 37 °C with 5% CO_2. Harvested cells were measured, and a sample containing 10^6 cells was

pelletized in the culture media. The supernatant was carefully eliminated, and the pellet was kept at −80 °C until use. Telomerase was isolated from the cells employing CHAPS lysis buffer.[22,27] Cell pellets (10^6 cells) were immersed in 200 μL of ice-cold 1× CHAPS lysis buffer (50 mM Tris-HCl (pH 7.4), 110 mM NaCl, 1% CHAPS, 5 mM EDTA) and then preserved on ice for 60 minutes. The lysate was centrifuged at 12 000 rpm for 20 minutes at 4 °C, and 160 μL of the supernatant was transferred to a new tube. The resultant extract was rapidly aliquoted, flash-frozen in liquid nitrogen, and then preserved at −80 °C until use.

2.3 Gold nanoparticle preparation

Au nanoparticles (AuNPs) were chemically synthesized by reducing gold ions (Au^{3+}) to gold atoms (Au^0) in the presence of citrate.[22] 10 mL of 1.0 mM $HAuCl_4$ was briefly heated to its boiling point while stirring. After boiling, 1.0 mL of 38.8 mM trisodium citrate was quickly added to the reaction solution. The resulting solution was left boiling for 5 minutes under constant stirring to complete the citrate reduction of the gold ions. After that, the solution was agitated for approximately 30 minutes until it cooled down. The colloidal gold was filtered using a 0.22 μm filter to eliminate aggregated nanoparticles. It was then characterized by employing a UV-vis spectrophotometer (Thermo Scientific™ Varioskan™ LUX Multimode Microplate Reader, Thermo Fisher Scientific). The shape, size, and homogeneity of the gold nanoparticles were evaluated using a Zetasizer Nano-ZS (Malvern PANalytical) and high-resolution transmission microscopy (HR-TEM) on a JEM3010 instrument with a voltage setting of 300 kV. The citrate-reduced AuNPs synthesized here are consistent with those used in the previous aggregation-based telomerase sensing study by Huyen *et al.* (2025), enabling a direct comparison between the aggregation and nanozyme signal transduction strategies.[33]

2.4 Evaluation of the catalytic activity of bare and DNA-coated colloidal gold nanoparticles

In this study, the catalytic activity of colloidal gold AuNPs was exploited based on the study by Huyen *et al.* (2025) to develop the nanoparticle-based colorimetric biosensor.[33] To demonstrate the peroxidase-like catalytic activity of the citrate-capped Au nanoparticles for telomerase detection, 3,3′,5,5′-tetramethylbenzidine (TMB), a peroxidase substrate, was exploited to evaluate their activity. Furthermore, to test the hypothesis that the surface coating of gold nanoparticles with elongated primers leads to the suppression of their peroxidase-like catalytic activity, the catalytic activity of AuNPs was tested under different conditions. In brief, 100 μL of 10 nM colloidal gold was mixed with TS primer (ssDNA)/hybrid DNA duplex between TS primer and complementary sequence (dsDNA) (5 μL, 10 μM). Next, the mixture was incubated for 20 min at room temperature to allow DNA to coat the gold surface completely. Afterward, the bare and DNA-coated AuNPs were incubated with 10 μL of 1.0 mM TMB/0.3% H_2O_2 solution for 5 min at room temperature. The catalytic activity of the colloidal gold nanoparticles was evaluated *via* visible inspection and UV/Vis

absorption spectral measurement (Varioskan™, Thermo Scientific).

2.5 Colorimetric nanoplasmonic biosensor for the measurement of telomerase activity

The telomerase extension reaction and exonuclease III-assisted processing strategy employed in this study follow the same upstream biochemical framework as our previously reported aggregation-based assay, while the downstream signal readout is fundamentally different.[33]

2.5.1 Telomerase extension reaction. In this research, CHAPS buffer solution was used to dilute the cell extracts. MCF-7 cells were counted and 10^6 cells were lysed to generate a stock cell extract. Serial dilutions of this stock lysate were prepared using CHAPS buffer to obtain samples corresponding to 10^1 to 10^6 cell equivalents. In all experiments, the reported cell number refers to the number of cell equivalents per reaction. A fixed volume of 2 μL of each diluted lysate was added to the telomerase extension reaction. To evaluate the analytical sensitivity of the proposed biosensor, 2 μL of MCF-7 cell extract with various concentrations ranging from 0 to 10^6 was subjected to incubation with 1 μL of TS primer (100 pM) and 2 μL of dNTPs (7.5 mM) in 10 μL of reaction buffer (150 mM NaCl, 50 mM Tris-HCl, 1 mM $MgCl_2$, 10 mM KCl, pH 7.4) at 37 °C for 1 hour. The negative controls were performed using the heated MCF-7 extract and normal human fibroblast cells. To demonstrate that there is no telomere in the other components of the reaction mixture, the reaction was performed in the absence of TS primer. The lack of cell extract in the elongation reaction was used to confirm that the other components in the reaction mixture did not lengthen the primer. In this case, the lysis CHAPS buffer was utilized as a blank sample. To confirm the elongation of the TS primer, the reaction mixtures were verified by agarose gel electrophoresis. Specifically, we used 1% agarose gel with GelRed for testing. Reaction mixtures consisting of 5 μL of the telomerase extension product and 1 μL of 6× GelRed were subjected to electrophoresis at 100 V for 40 minutes. Following separation, the gel was imaged using an Azure C300 Imaging System. The loading volume and sample concentration were carefully adjusted to ensure sufficient signal intensity.

2.5.2 Hybridization between elongated primer and TS complementary sequence, and the digestion of hybrid DNA duplex by exonuclease III. After the primer was elongated by telomerase from the cell extracts, the elongated TS primer was hybridized with the complementary sequence by mixing 13 μL of the elongated primer with the complementary sequence (1 μL, 100 pM) in the hybridization buffer (150 mM NaCl, 50 mM Tris–HCl, 1 mM $MgCl_2$, 10 mM KCl, pH 7.4) to form the hybrid DNA duplex. The reaction mixture was incubated at 90 °C for 2 minutes, and then at 60 °C for 30 minutes. Then, exonuclease III (Exo III) (1 μL, 10 U per μL) was added to the reaction mixture to remove nucleotides from the 3′ blunt-end of the hybrid dsDNA, and the resultant solution was then incubated at 37 °C for 30 minutes.

2.5.3 Colorimetric detection of telomerase activity based on the catalytic activity of Au nanoparticles. After the digestion

of hybrid DNA duplex by Exo III, the telomerase activity of the cell extracts was evaluated based on the peroxidase-like catalytic activity of the plasmonic nanoparticles, which can oxidize the 3,3′,5,5′-tetramethylbenzidine (TMB) substrate in the presence of hydrogen peroxide. In a detecting proof-of-concept assay, 12 µL of the reaction mixture was mixed with 100 µL of citrate-capped AuNPs and incubated for 10 minutes at room temperature. Subsequently, 10 µL of 1.0 mM TMB/0.3% H_2O_2 solution was added to the mixture. After incubating at room temperature for 5 minutes, the solution was examined by visible inspection and UV/Vis absorption spectral measurement (Varioskan™, Thermo Scientific, USA). All data were obtained from at least three independent assessments. Compared to the aggregation-based plasmonic readout reported previously, the nanozyme-based catalytic detection strategy employed here enables active signal amplification through continuous TMB oxidation, resulting in improved analytical sensitivity and a lower detectable cell-equivalent number.[33]

2.6 Evaluation of the generality of designed plasmonic nanosensor for telomerase analysis

Many reports demonstrated that telomerase activity is overexpressed in most cancer cells, germline cells and stem cells, and their proliferation requires overexpression of telomerase to prevent telomere shortening, which occurs during cell division.[28] To demonstrate that the proposed method is universal for the detection of telomerase activity in tumor cells, various cell lines were tested. These cell lines include human breast cancer cells (MCF-7), mouse colon cancer cells (C26), human liver cancer cells (HepG2) and mouse fibroblast cells (L929). Normal human fibroblast cells and a blank sample were used as the controls for telomerase analysis.

2.7 Statistical analysis

In this research, one-way ANOVA was utilized to evaluate the statistically significant difference between test groups. If the p-value was less than 0.05, the difference was considered statistically significant. All absorbance measurements were performed in triplicate as technical replicates within the same assay run. The data points are shown as the mean $\pm$ standard deviation (SD) of the data set.

3 Results and discussion

The working principle of the proposed sensing approach for the colorimetric detection of telomerase activity in cell lysates is demonstrated in Fig. 1. As shown in this figure, the sensing approach exploits the telomere extension activity of telomerase combined with the specific cleavage activity of exonuclease III and intrinsic peroxidase-like catalytic activity of plasmonic nanoparticles. In this study, colloidal Au nanoparticles were exploited as a catalyst for colorimetric biosensing. The gold nanoparticles demonstrate strong peroxidase-mimicking activity, catalyzing the oxidation of 3,3′,5,5′-tetramethylbenzidine (TMB) in the presence of hydrogen peroxide (H_2O_2) to produce 3,3′,5,5′-tetramethylbenzidine diamine
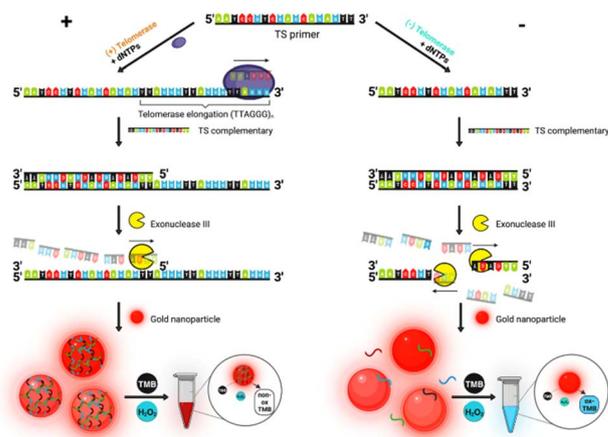

Fig. 1 Overall framework illustrating the principle of the gold nanoparticle-based colorimetric biosensor for detecting the telomerase activity in cell lysates based on the peroxidase-mimicking gold nanozyme.

(oxidized TMB), a blue-colored product. The peroxidase-like activity of colloidal gold originates from the interaction of the gold surface with TMB, a substrate of peroxidase.[26,31] Hence, the peroxidase-like catalytic activity of AuNPs is suppressed due to the shielding effect when the Au nanoparticles are coated with DNA or protein. More specifically, single-stranded DNA (ssDNA) exhibits strong affinity toward the AuNP surface via electrostatic interaction between the positively charged bases of ssDNA and the negative charge of the gold surface.[37] The adsorbed ssDNA forms a passivating layer, which sterically and electronically blocks the access of TMB and H_2O_2 to the catalytically active gold surface sites, thereby suppressing electron transfer and inhibiting the peroxidase-like activity of AuNPs.[38] In the presence of telomerase from the cell lysates, it catalyzes the extension of the telomerase substrate (TS primer) to produce extension products containing telomeric repeats (TTAGGG)$_n$. Then, the elongated telomere is hybridized with the complementary strand of TS primer, which leads to the formation of double-stranded DNA (hybrid DNA duplex) with a 3′ single-stranded overhang (3′-OH) and a blunt end. The subsequent DNA duplex becomes a target for cleavage of exonuclease III (Exo III), which is known as a double-stranded DNA (dsDNA)-specific exonuclease that can catalyze the stepwise removal of mononucleotides from the 3′ blunt-end of dsDNA.[29] This allows the single strands of elongated primers to liberate in the solution, and these elongated primers in turn adsorb on the Au nanoparticle surface via electrostatic interaction, which helps to block the gold surface and suppress its intrinsic peroxidase-like activity. As a result, the colloidal gold maintains its ruby red color in the presence of TMB/H_2O_2. In the absence of telomerase in the cell extract, the TS primer is not extended. As a result, the hybrid DNA duplex is formed with two blunt-ends, and it is completely degraded by Exo III. In this case, the uncoated Au nanoparticles can catalyze the oxidation of TMB in the presence of H_2O_2 to produce a blue-colored product, which can be detected by the naked eye or low-cost handheld absorbance spectrophotometer.
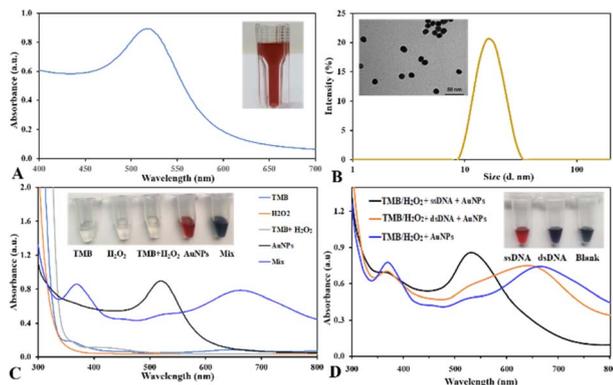
Fig. 2 Characterization and catalytic activity of synthesized Au nanoparticles: (A) UV-vis spectrum of the Au nanostructures (inset: photograph revealing the ruby red color of the colloidal Au); (B) size distribution and morphology (inset image) of the Au nanostructures with a diameter of ~15 nm, as revealed by the Zetasizer Nano and JEOL JEM-1400 TEM (scale bar: 50 nm) instruments; (C) typical UV-vis spectra and photographs (inset) demonstrating the peroxidase-like catalytic activity of Au nanostructures for the oxidation of TMB in the presence of H_2O_2; and (D) UV-vis spectra and photographs (inset: color images of the respective samples) verifying the capability of ssDNA to suppress the peroxidase-mimicking activity of Au nanoparticles when ssDNA absorbs on the gold surface.

To investigate the optical response of the nanoplasmonic biosensor for telomerase activity detection, Au nanoparticles (AuNPs) were chemically synthesized by reducing hydrogen tetrachloroaurate with sodium citrate, employing the Turkevich method with minor modifications.[22] As shown in Fig. 2, this method yielded ruby-red colloidal nanoparticles with a diameter of ~15 nm diameter, as disclosed by a Zetasizer Nano and transmission electron microscope. As shown in Fig. 2A, the colloidal gold nanoparticles exhibit a strong resonant peak at 520 nm, which is assigned to the localized surface plasmon resonance (LSPR) of Au nanoparticles. The concentration of prepared AuNPs was ~10 nM ($OD_{520nm} \approx 2.0$), which was estimated by their average diameter and extinction coefficient, as described in the previous study.[32] The analysis using Zetasizer revealed that the hydrodynamic size of the Au nanoparticle was 15.4 ± 1.5 nm with a PDI of 0.052 ± 0.01 (Fig. 2B), and the its zeta potential was found to be -36.7 ± 7.5 mV. These results showed that the Au nanoparticles are fairly homogenous and quite stable. To demonstrate the catalytic activity of the citrate-capped Au nanoparticles for the colorimetric detection of telomerase, TMB, a peroxidase substrate was utilized to check their catalytic activity. Fig. 2C indicates that the mixture of 1 mM TMB and 0.3% H_2O_2 changed to a vivid blue color due to the presence of colloidal gold, which demonstrates the remarkable peroxidase-like catalytic activity of the synthesized Au nanoparticles, while only TMB or TMB/H_2O_2 solution could not be changed into the oxidized state of TMB on its own. The oxidation of TMB in the presence of H_2O_2 catalyzed by colloidal gold is demonstrated by the formation of charge transfer complexes with two distinct absorption peaks at 370 nm and 650 nm, and the color intensity of the oxidized TMB is in accordance with the catalytic activity of the Au nanoparticles.[30,31] To test the

hypothesis that the nanoparticle surface coating with ssDNA leads to the suppression of its catalytic activity, the catalytic activity of AuNPs was tested under different conditions. As shown in Fig. 2D, in the presence of ssDNA, the gold nanoparticles keep their red dispersed state and the resonance peak at 520 nm due to the absorption of ssDNA on their surface, resulting in the inhibition of the intrinsic peroxidase-like catalytic activities of the gold nanozymes. This inhibition arises because the adsorbed ssDNA effectively passivates the AuNP surface, preventing interaction between the nanozyme active sites and the TMB/H_2O_2 substrate system. In the case of the DNA duplex, the helical structure of dsDNA prevents it from adhering to the surface of AuNPs; hence, it cannot block the peroxidase-like catalytic activities of the Au nanoparticles. As a result, the TMB/H_2O_2 and gold colloidal solution turns blue color with two major absorption peaks at 370 and 650 nm, which are characteristic of oxidized TMB. According to these results, it can be said that the high stability and strong catalytic activity of colloidal gold as well as the capacity of ssDNA to restrain the peroxidase-like activity of AuNPs can be exploited for the design of colorimetric assays for the detection of telomerase activity.

To verify the feasibility of the proposed biosensor for the colorimetric detection of telomerase activity using the peroxidase-like catalytic activity of colloidal gold, we examined the specificity of this assay by conducting trials with a blank sample, negative control and positive control (MCF-7 cells). Before testing the performance of the sensing approach, we first confirmed the telomerase activity of the test samples with telomerase substrate using agarose gel electrophoresis. In this case, the telomerase extension reaction was carried out without the TS primer to show that the primer was not lengthened in this situation. The absence of cell extract in the reaction was
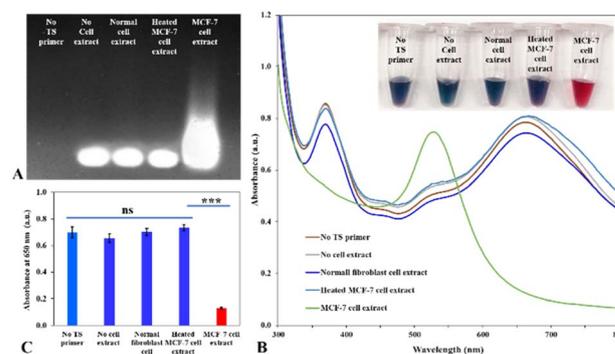

Fig. 3 Specificity of the colorimetric assay for the detection of telomerase activity based on the catalytic activity of AuNPs: (A) agarose gel electrophoresis of the telomere extension solutions by the MCF-7 cell extract in comparison with other controls including TS primer-free (no TS primer), cell extract-free (no cell extract), normal fibroblast cell extract and heated MCF-7 cell extract; (B) UV-vis spectra of the samples measured from 300 to 800 nm; and (C) absorbance at 650 nm of the respective samples. The error bar displays the standard deviation and ANOVA test results (n.s.: $P > 0.05$ and ***$P < 0.01$) from the triplicates of each response. Inset: photograph displaying the colorimetric responses of the biosensor to the corresponding samples.

also used to prove that the TS primer was not extended by the other components of the reaction. As clearly indicated in Fig. 3A, in the absence of TS primer and cell extract, the gel showed no visualization or telomere elongation. This indicated that neither the cell extract nor the reaction buffer (blank) contained contaminants. In the absence of telomerase in the normal fibroblast cell extract or inactivation of telomerase in the heated MCF-7 cell extract, no extension product was found in these cases, and the gel just showed the band of TS primer with its length of 18 nucleotides. This proved that the test was both uncontaminated and unaffected by outside influences. Regarding the MCF-7 cell extract, the agarose gel showed a bright smear, which demonstrated the extension of the primer by the telomerase in the cell extract and the extension product had telomeres with various lengths. These results indicated that the extension reaction mixtures from the blank sample, negative control and positive control were suitable for testing the specificity of the proposed biosensor for the detection of telomerase activity. Fig. 3B displays the colorimetric and spectral responses of the biosensor to the corresponding samples. As shown in the figure, in the absence of primer, without cell extract, normal cell extract, and heated MCF-7 cell extract, the colloidal gold solution changed from red to blue when TMB/H_2O_2 was added to the mixture. In these cases, the primer was not elongated, and the DNA duplex was formed with two blunt-end. This enables the complete digestion of dsDNA by Exo III into dNMPs. Consequently, the final product was incapable of protecting and inhibiting the peroxidase catalytic activity of colloidal gold. Thus, the blue color of oxidized TMB was produced with two major absorption peaks at 370 and 650 nm, which demonstrates the oxidized state of TMB. In contrast, in the presence of telomerase in the MCF-7 cell extract, a prolonged response was observed between telomerase and the TS primer. The hybrid product of the TS primer and the TS complementary sequence was a DNA duplex with 3′ overhangs. The 3′ end of the duplex DNA was subsequently degraded by the Exo III enzyme into dMNPs and single strands of elongated primers. These elongated primers coated the surface of the AuNPs, which inhibited their peroxidase-like activity and maintained the red color of the solution in the presence of TMB and H_2O_2. In this scenario, only the sample containing MCF-7 cell extract was capable of maintaining the original ruby red color and the initial absorption peak of AuNPs at 520 nm, while the negative controls turned blue color and two absorption peaks appeared at 370 nm and 650 nm. Consequently, the telomerase activity could be evaluated based on the change in the color change and absorption of the reaction solution. In this study, the change in absorption at 650 nm was used to evaluate the telomerase activity of the cell lysate. Fig. 3C compares the relationship between the absorbance at 650 nm and telomerase activity from the MCF-7 cell extract, normal fibroblast cell extract, heated MCF-7 cell extract and control samples. The results demonstrated that the absorbance at 650 nm of the sample containing MCF-7 cell extract was remarkably lower than that of the normal cell lysate and control samples. This result proved that the primer elongated by telomerase from the MCF-7 cell adsorbs on the nanoparticle surface and suppresses

its intrinsic peroxidase-like activity. The statistical analysis revealed that the difference between the MCF-7 sample and control samples was statistically significant. Importantly, the absence of signal suppression in the normal fibroblast cell extracts and heated MCF-7 lysates indicates that other cellular components, including non-specific proteins, endogenous nucleases, and redox-active biomolecules, do not interfere with the assay response. This high specificity arises from the requirement of active telomerase to generate elongated telomeric ssDNA, which is the only species capable of adsorbing onto the AuNP surface and suppressing nanozyme activity. Consequently, the background oxidation of TMB caused by the matrix components is minimized under the optimized reaction conditions. These results proved that the sensing approach was capable of detecting telomerase activity in cell lysates and in complex biological media.

To evaluate the analytical sensitivity of the proposed plasmonic nanosensor, different concentrations of MCF-7 cell lysate ranging from 0 to 10^6 were incubated with the TS primer in the reaction buffer for the analysis of telomerase activity. Fig. 4 depicts the colorimetric assay of the biosensor to detect telomerase activity at concentrations ranging from 10^0 to 10^6 MCF-7 cells compared to the blank. As shown in Fig. 4A, the gel electrophoresis result demonstrated that the quantity and length of elongated telomeres from the elongation process increased when the concentration of MCF-7 cell lysate added to the reaction mixture increased from 10^0 to 10^6. In this case, the increased amount of elongated primers assists in inhibiting the catalytic activity of AuNPs. Consequently, the color of the reaction solution changed linearly from blue to wine red as the cell concentration increased from 10^0 to 10^6 (Fig. 4B). It is easy to realize that the cell extract with a concentration of ~10^2 cells can be detected with the naked eye. Fig. 4B also demonstrates
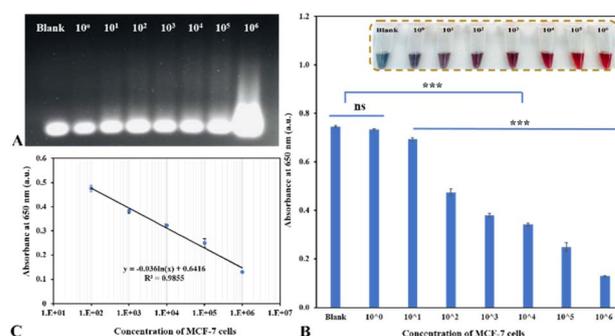

Fig. 4 Colorimetric assay for detecting the telomerase activity of MCF-7 cells at various concentrations from 0 to 10^6 cells: (A) gel electrophoresis of the telomere extension solutions of the corresponding samples; (B) normalised absorbance at 650 nm as a function of the concentration of MCF-7 cells; and (C) linear curve demonstrating the relationship between the concentration of MCF-7 cells and their absorbance at 650 nm. The error bar displays the standard deviation and ANOVA test results (n.s.: $P > 0.05$ and ***$P < 0.01$) from the triplicates of each response. Inset: photograph illustrating the color shift from blue to wine red as the concentration of the cell extract increases. Each data point represents the mean ± SD of three technical replicates.

a decrease in peak absorbance at 650 nm as the concentration of MCF-7 cells increases up to 10^6 cells. The normalised absorbance at 650 nm in the sample containing 10^0 MCF-7 cells and blank sample did not differ significantly ($P > 0.05$). However, the absorbance differed considerably ($P < 0.01$) between the sample with 10^1 cells and the blank sample. Fig. 4C shows the linear fitting between the absorbance at 650 nm and concentration of MCF-7 cell lysate, where this absorption was linear in the concentration range of 10^2 to 10^6 cells. The resulting linear regression equation is $y = -0.036 \ln(x) + 0.6416$ ($R^2 = 0.9855$), where y and x represent the absorbance at 650 nm and the concentration of MCF-7 cells, respectively. The detection limit was computed using the formula $3\sigma/s$, where $\sigma = 0.00397$ represents the standard deviation of the blank sample and s is the slope of the linear regression equation (0.036). As a consequence, this assay has a detection limit of ~0.3 cells, which is lower than that of most of the PCR-free methods.[9–15] To further contextualize the analytical performance of the proposed assay, a comparison with representative PCR-free telomerase detection strategies reported in the literature was performed. These include nanoparticle aggregation-based colorimetric assays, CRISPR-Cas12a-based visual detection, electrochemical biosensors, and DNAzyme-based photoelectrochemical platforms. Key analytical and practical parameters, including signal transduction mechanism, linear range, detection limit, and assay time, are summarized in Table 1. As summarized in Table 1, the proposed nanozyme-based assay achieves a detection limit of approximately 0.3 cells using spectrophotometric readout, which is comparable or superior to most reported PCR-free telomerase detection methods. Compared with nanoparticle aggregation-based assays, the present method offers improved sensitivity (LOD ~0.3 cells *versus* ~5 cells), owing to the exploitation of the intrinsic peroxidase-like catalytic activity of dispersed Au nanoparticles rather than aggregation-induced optical shifts.[33] In contrast to electrochemical and photoelectrochemical biosensors, which typically require specialized electrodes, light sources, or electrochemical workstations, the proposed assay relies on a simple colorimetric readout, which can be performed by the naked eye or using a low-cost spectrophotometer.[35,36] Moreover, unlike CRISPR-based assays, which depend on programmable nucleases and crRNA design, this method avoids enzymatic signal
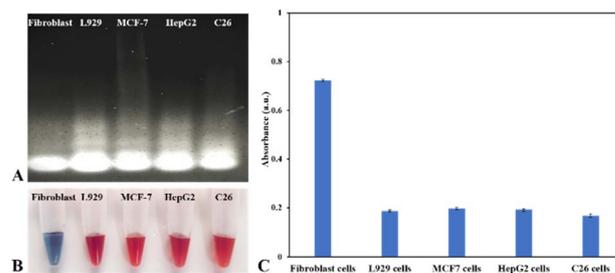

Fig. 5 Colorimetric assay for the evaluation of telomerase activity in different cell lines: (A) agarose gel electrophoresis image to examine the telomerase elongation activity of different cell lines; (B) photograph illustrating the color shift from blue to wine red as the concentration of cell extract increases; and (C) absorbance change at 650 nm of the designed biosensor for the telomerase activity analysis of different cell lines.

amplification and complex reagent preparation.[34] Collectively, the designed nanoplasmonic biosensor demonstrates clear advantages in terms of simplicity, low cost, reliability, analytical sensitivity, assay time, and suitability for point-of-care diagnostics, without the need for sample pretreatment or nucleic acid amplification.

To demonstrate the universality and reliability of the designed biosensor for the analysis of telomerase activity, the telomerase activity of various cell lines, including tumor cells and normal cells, was tested. As demonstrated in Fig. 5, all types of cancer cells (MCF-7, C26, HepG2) exhibit a strong signal for the catalytic activity of telomerase. In the case of the L929 cell line, a fibroblast cell line from subcutaneous connective tissue of mice, the result indicated that this cell line shows high telomerase activity. The detectable telomerase-associated signal observed in the L929 cells may be related to the altered proliferative or immortalization-associated characteristics reported for some fibroblast cell lines after extended passaging; however, this interpretation remains speculative and requires independent biological validation. Regarding the blank sample and normal fibroblast cells, they did not cause any colorimetric and spectral signal due to the scarcity of telomerase. These results were well consistent with the gel electrophoresis result, which was used to check the telomerase elongation activity of different cell lines. This suggests that our sensing approach has very high

Table 1 Comparison of representative PCR-free telomerase detection platforms in terms of their analytical performance

Platform	Linear range	Detection limit (LOD)	Time for analysis	Ref.
TRAP based on TS primer-modified AuNPs	—	5 cells	1.5–3 h	9
Nanosensor using the interaction between telomere and telomerase	10^2–10^5 cells	10 cells	20–24 h	22
Visual detection of telomerase activity using AuNP aggregation	10^2–10^6 cells	5 cells	~3 h	33
CRISPR-Cas12a telomerase assay	—	18 cells	~1.5 h	34
Electrochemical biosensor using SNAs AuNP-triggered mimic HCR dual signal amplification	10^1–10^4 cells	2 cells	—	35
Photoelectrochemical biosensor based on DNAzyme-mediated biodeposition	10^1–10^5 cells per mL	3 cell per mL	—	36
Visual detection of telomerase activity using the peroxidase-mimicking activity of nanogold	10^2–10^5 cells	~0.3 cells	~3 h	Our work

specificity, and it can be exploited for early clinical diagnostics and anticancer drug development.

While the present study demonstrates the sensitive and selective detection of telomerase activity using cultured cell lysates, translation to real clinical samples such as blood or serum will require additional considerations. Clinical matrices contain abundant proteins, enzymes, and redox-active species that may interfere with nanozyme activity or contribute to the background oxidation of TMB. Matrix effects may also influence ssDNA adsorption on AuNP surfaces and thus affect the signal reproducibility. To address these challenges, future studies may incorporate sample pretreatment steps such as dilution, protein depletion, or isolation of circulating tumor cells prior to analysis. Importantly, the label-free and amplification-free nature of the proposed nanozyme-based sensing strategy provides a flexible foundation for adaptation to clinically relevant sample formats.

4 Conclusions

In summary, we reported a simple, fast, label-free and ultrasensitive method for the POC colorimetric detection of telomerase activity in cell lysates, which exploits the telomere elongation activity of telomerase, selective cleavage of exonuclease III and peroxidase-mimicking catalytic activity of gold nanozymes. Using MCF-7 cells as a model, the nanosensor successfully detected telomerase activity in samples containing as few as $\sim$0.3 cells, with a broad linear dynamic range from 10^2 to 10^6 cells. Importantly, this approach eliminates the need for thermal cycling for DNA amplification, addressing the limitations of PCR-free assays and overcoming the drawbacks of traditional TRAP methods, which are time-consuming, challenging to quantify, and prone to PCR-related artifacts. While the present study demonstrates robust intra-assay repeatability and analytical sensitivity at the proof-of-concept level, further evaluation of the inter-assay reproducibility and validation using independent assay runs and clinical samples will be required to fully establish the robustness of the platform for translational applications. One limitation of the present study is that nonspecific ssDNA adsorption onto AuNPs was not independently evaluated using controls such as unextended TS primers, random ssDNA of comparable length, or telomerase reactions lacking dNTPs. Future studies will systematically address these controls to further clarify the nanozyme-DNA interactions and strengthen the assay specificity, particularly in complex biological matrices. Besides, another limitation of this study is that the dependence of the signal on exonuclease III activity was not independently validated using explicit "no Exo III" or Exo III dose–response controls; future work will systematically address these experiments to further confirm the proposed amplification and primer-release mechanism. Taken together, addressing these limitations is expected to further enhance the robustness and translational potential of the proposed platform. The proposed approach offers a sensitive and practical colorimetric approach for the colorimetric detection of telomerase activity and shows promise as a foundational sensing strategy for telomerase analysis, with potential for future adaptation toward circulating tumor cell detection and point-of-care applications following further validation in clinical samples.

Author contributions

Dr Phuoc Long Truong was responsible for conceptualization, methodology, supervision, and writing—original draft preparation. Le Thi Hoang Uyen contributed to research design, data analysis, data curation, and manuscript preparation. Cam-Duyen Thi Vo prepared and revised the initial draft of the manuscript. All authors reviewed the manuscript and approved the final version.

Conflicts of interest

The authors disclose no conflicts of interest.

Data availability

The data supporting this study are included within the article and/or its supplementary information (SI). Supplementary information is available. See DOI: https://doi.org/10.1039/d5ra08471g.

Notes and references

1 E. H. Blackburn and K. Collins, *Cold Spring Harbor Perspect. Biol.*, 2011, **3**(5), a003558.

2 J. W. Shay and W. E. Wright, *Nat. Rev. Genet.*, 2019, **20**(5), 299–309.

3 N. W. Kim, M. A. Piatyszek, K. R. Prowse, C. B. Harley, M. D. West, P. L. Ho and J. W. Shay, *Science*, 1994, **266**(5193), 2011–2015.

4 D. Hanahan and R. A. Weinberg, *cell*, 2000, **100**(1), 57–70.

5 J. W. Shay and S. Bacchetti, *Eur. J. Cancer*, 1997, **33**(5), 787–791.

6 M. Armanios and E. H. Blackburn, *Nat. Rev. Genet.*, 2012, **13**(10), 693–704.

7 N. W. Kim and F. Wu, *Nucleic Acids Res.*, 1997, **25**(13), 2595–2597.

8 Y. Cong and J. W. Shay, *Cell Res.*, 2008, **18**(7), 725–732.

9 Y. Xiao, K. Y. Dane, T. Uzawa, A. Csordas, J. Qian, H. T. Soh and K. W. Plaxco, *J. Am. Chem. Soc.*, 2010, **132**(43), 15299–15307.

10 R. Freeman, E. Sharon, C. Teller, A. Henning, Y. Tzfati and I. Willner, *ChemBioChem*, 2010, **11**(17), 2362–2367.

11 H. Wang, S. Wang, H. Wang, Y. Liang and Z. Li, *Talanta*, 2023, **253**, 123999.

12 E. Sharon, E. Golub, A. Niazov-Elkan, D. Balogh and I. Willner, *Anal. Chem.*, 2014, **86**(6), 3153–3158.

13 W. J. Wang, J. J. Li, K. Rui, P. P. Gai, J. R. Zhang and J. J. Zhu, *Anal. Chem.*, 2015, **87**(5), 3019–3026.

14 L. Liu, D. Wu, S. Zhen, K. Lu, X. Yi and Z. Sun, *Sens. Actuators, B*, 2021, **334**, 129659.

15 M. Chehelgerdi, M. Chehelgerdi, O. Q. B. Allela, R. D. C. Pecho, N. Jayasankar, D. P. Rao and R. Akhavan-Sigari, *Mol. Cancer*, 2023, **22**(1), 169.

16 P. Martínez and M. A. Blasco, *J. Cell Biol.*, 2017, **216**(4), 875.

17 C. C. Chang, C. P. Chen, T. H. Wu, C. H. Yang, C. W. Lin and C. Y. Chen, *Nanomaterials*, 2019, **9**(6), 861.

18 P. L. Truong, N. T. T. Thao, H. T. Le Huyen and T. H. Nguyen, *J. Nanomater.*, 2022, **2022**(1), 1107081.

19 Z. Yu, F. Jiang, C. Hu and B. Tang, *Chem. Commun.*, 2021, **57**(31), 3736–3748.

20 P. N. A. Thu, N. H. Men, C. D. T. Vo, V. Van Toi and P. L. Truong, *Anal. Methods*, 2024, **16**(18), 2913–2920.

21 B. Das, J. L. Franco, N. Logan, P. Balasubramanian, M. I. Kim and C. Cao, *Nano-Micro Lett.*, 2021, **13**(1), 193.

22 X. Ma, P. L. Truong, N. H. Anh and S. J. Sim, *Biosens. Bioelectron.*, 2015, **67**, 59–65.

23 Z. Yu, F. Jiang, C. Hu and B. Tang, *Chem. Commun.*, 2021, **57**(31), 3736–3748.

24 H. Li and L. Rothberg, *Proc. Natl. Acad. Sci. U. S. A.*, 2004, **101**(39), 14036–14039.

25 N. Farkhari, S. Abbasian, A. Moshaii and M. Nikkhah, *Colloids Surf., B*, 2016, **148**, 657–664.

26 T. K. Sharma, R. Ramanathan, P. Weerathunge, M. Mohammadtaheri, H. K. Daima, R. Shukla and V. Bansal, *Chem. Commun.*, 2014, **50**(100), 15856–15859.

27 M. A. Piatyszek, N. W. Kim, S. L. Weinrich, K. Hiyama, E. Hiyama, W. E. Wright and J. W. Shay, *Methods Cell Sci.*, 1995, **17**(1), 1–15.

28 M. Liu, Y. Zhang, Y. Jian, L. Gu, D. Zhang, H. Zhou and Z. X. Xu, *Cell Death Dis.*, 2024, **15**(1), 90.

29 Y. Shen, H. Yuan, Z. Guo, X. Q. Li, Z. Yang and C. Zong, *Biosensors*, 2023, **13**(6), 581.

30 M. Drozd, M. Pietrzak, P. G. Parzuchowski and E. Malinowska, *Anal. Bioanal. Chem.*, 2016, **408**(29), 8505–8513.

31 C. McVey, N. Logan, N. T. Thanh, C. Elliott and C. Cao, *Nano Res.*, 2019, **12**(3), 509–516.

32 W. Haiss, N. T. Thanh, J. Aveyard and D. G. Fernig, *Anal. Chem.*, 2007, **79**(11), 4215–4221.

33 H. T. Le Huyen, V. T. C. Duyen and P. L. Truong, *Anal. Methods*, 2025, **17**(1), 162–169.

34 X. Gu, T. Zhang, H. Yao, F. Guo, C. Yang, H. Xu, X. he, Z. ma, X. Zhang, S. Yu, R. An and F. Wang, *Biosens. Bioelectron.*, 2025, 118241.

35 W. J. Wang, J. J. Li, K. Rui, P. P. Gai, J. R. Zhang and J. J. Zhu, *Anal. Chem.*, 2015, **87**(5), 3019–3026.

36 Y. Wang, L. Li, S. Ge, L. Zhang, X. Wang and J. Yu, *ACS Sens.*, 2023, **8**(9), 3538–3546.

37 M. Ramezani, N. M. Danesh, P. Lavaee, K. Abnous and S. M. Taghdisi, *Biosens. Bioelectron.*, 2015, **70**, 181–187.

38 P. Weerathunge, R. Ramanathan, R. Shukla, T. K. Sharma and V. Bansal, *Anal. Chem.*, 2014, **86**(24), 11937–11941.